Sports Engineering (2024) 27:16
https://doi.org/10.1007/s12283-024-00456-6

ORIGINAL ARTICLE

Three-dimensional golf clubhead-ball impact models for drivers and irons

Adam Caldwell[1] · **John McPhee**[1]

Accepted: 9 March 2024 / Published online: 17 April 2024

Abstract
Impact models are an important tool for golf equipment design as they allow for computer simulations to evaluate and optimize performance. There are several published driver impact models for this purpose. However, existing impact models have no or limited experimental validation to support their conclusions. The aim of this research was to extend several impact models from the literature to predict three-dimensional driver impacts and, for the first time, iron impacts. The accuracy of these models was evaluated using experimental data. Two impulse-momentum and three continuous contact models were applied to create dynamic models to predict driver and iron golf shots. While finite element models are used to design golf clubs, they were not considered here due to their high computational requirements. For modeling driver impacts, an adjusted IM model was the most accurate at predicting ball launch conditions. Ball speed was the most accurate launch condition with a mean absolute error of 1%. The error for vertical launch angle and backspin was less than 10%. However, the error for sidespin and horizontal launch angle (azimuth) was between 30 and 50%. For modeling 7-iron shots, a two-layer ball with a volumetric normal force model was the most accurate of the models considered. The experimental error for ball speed was 2%. The remaining errors were similar to the driver model.

Keywords Dynamics · Modeling

1 Introduction

Modern golf club design increasingly uses advanced computer simulations to optimize new designs. Over the last 30 years, the average driving distance among professional players has increased by more than 30 yards [1]. These performance gains are largely associated with the equipment, as they coincide with the major design innovations in clubs and balls [2, 3]. In the last decade, the innovations developed for drivers have trickled down to irons [3]. There are several published models of driver-ball impacts, but very few of these models have been validated using motion capture data collected from elite golfers [4, 5]. Furthermore, there are no published three-dimensional (3D) models of iron-ball impacts. This research builds on existing impact models and applies these methods to predict driver and iron club performance.

The models presented here are divided into two classes. The first class is referred to as impulse-momentum (IM) models. These models use the impulse-momentum principle to predict the velocities of the clubhead and ball after impact. In this paper, an adjusted IM model is tuned specifically for driver impacts and, for the first time, developed for iron impacts. In addition, a variable slip IM model is extended to 3D and used to predict driver and iron impacts. This model replaces the pure rolling condition assumed by most IM-based models. The second class is referred to as continuous models, which explicitly model the time-varying contact forces during the collision. Three continuous impact models are extended to model the collision between a golf ball and clubhead. First, a volumetric normal force model with a two-layer ball model is tuned. Next, a damping term is added to a Hertzian-based contact model that uses a tangentially compliant sphere. Lastly, a model that uses the contact area to predict the tangential force is developed. These three continuous contact models were used to predict both driver and iron impacts. Experimental data was used to evaluate

✉ Adam Caldwell
awcaldwell@uwaterloo.ca

John McPhee
mcphee@uwaterloo.ca

[1] Systems Design Engineering, University of Waterloo, Waterloo, ON, Canada

and compare the accuracy of all five impact models. While finite element (FE) models are continuous, they were not considered here due to their high computational requirements. The purpose of the work is to determine an impact model that can be combined with other models to predict the entire system including the golfer, club and ball. Previous researchers have developed models for the golf swing, flexible club shafts, and ball trajectories. These computer models take on the order of seconds to run; therefore, it is impractical to use an impact model that takes several orders of magnitude longer than the rest of the system. This is important as we expect to run these models thousands of times in optimization processes.

2 Methods

From the literature, two IM-based and three continuous impact models were considered. These five impact models were extended to model 3D driver and 7-iron shots. All models assume that the clubhead behaves as a free body during impact [6]. Each model begins with the ball and clubhead initial positions and velocities at the moment of impact. The following sections outline the impact models from literature and the modifications proposed here to predict 3D golf impacts.

2.1 Impulse-momentum models

IM models predict the launch conditions of the golf ball by applying the principles of linear and angular impulse-momentum. This requires several assumptions about the characteristics of the collision. First, IM models are discrete with respect to time, which implies that the collision is instantaneous. This leads to the assumption that neither body translates nor rotates during impact. Therefore, the contact between the clubhead and ball occurs at a single point. Furthermore, the changes in velocity are assumed to occur instantly. Finally, to model inelastic collisions, a coefficient of restitution (COR) is imposed along the axis normal to the clubface.

To construct the impact model, a system of equations is derived relating the velocities of each body before and after the collision. The ball and clubhead are modeled as free bodies as shown in Fig. 1. Each body has 3 translational and 3 rotational degrees of freedom. This gives 12 unknown velocity components after the collision. An impulse, $\vec{\mathbf{P}} = \int \vec{\mathbf{F}}\, dt$, is applied to each body at the point of impact as shown in Fig. 1. As per Newton's third law, a pair of impulses of equal magnitudes but opposite directions are applied to the ball and clubhead. Impulse is a vector quantity, bringing the total number of scalar unknowns to 15. The velocities are measured at the centre of gravity (CG) for each body. The reference frame $x'y'z'$ is located at the point of contact where x' is normal to the clubface.

The following equations describe the change in linear and angular velocity for the clubhead. In Eq. 1, m_c is the clubhead mass and $\vec{\mathbf{v}}_\mathbf{c}$ is the clubhead velocity. In Eq. 2, $\mathbf{I_c}$ is the inertia dyadic and $\vec{\boldsymbol{\omega}}_\mathbf{c}$ is the angular velocity of the clubhead. As shown in Fig. 1, $\vec{\mathbf{r}}_{\mathbf{CG-imp}}$ is a vector from the clubhead CG to the point of impact on the clubface.

$$m_c\vec{\mathbf{v}}_{\mathbf{c_i}} - \vec{\mathbf{P}} = m_c\vec{\mathbf{v}}_{\mathbf{c_f}} \tag{1}$$

$$\mathbf{I_c}\cdot\vec{\boldsymbol{\omega}}_{\mathbf{c_i}} - \vec{\mathbf{r}}_{\mathbf{CG-imp}}\times\vec{\mathbf{P}} = \mathbf{I_c}\cdot\vec{\boldsymbol{\omega}}_{\mathbf{c_f}} \tag{2}$$

Equations 1 and 2 are vector equations. This produces 6 scalar equations. Similarly, applying this process to the ball gives 6 additional equations. In Eq. 3, m_b is the mass and $\vec{\mathbf{v}}_\mathbf{b}$ is the velocity of the ball. In Eq. 4, $\mathbf{I_b}$ is the inertia dyadic and $\vec{\boldsymbol{\omega}}_\mathbf{b}$ is the angular velocity of the ball. Finally, $\vec{\mathbf{r}}_{\mathbf{ball}}$ is a vector from the ball CG to the point of impact.

$$m_b\vec{\mathbf{v}}_{\mathbf{b_i}} + \vec{\mathbf{P}} = m_b\vec{\mathbf{v}}_{\mathbf{b_f}} \tag{3}$$

$$\mathbf{I_b}\cdot\vec{\boldsymbol{\omega}}_{\mathbf{b_i}} + \vec{\mathbf{r}}_{\mathbf{ball}}\times\vec{\mathbf{P}} = \mathbf{I_b}\cdot\vec{\boldsymbol{\omega}}_{\mathbf{b_f}} \tag{4}$$

The right-hand side of Eqs. 1–4 are the respective momenta just after the collision and denoted by the subscript *f*, while the left-hand side includes the momenta just before impact

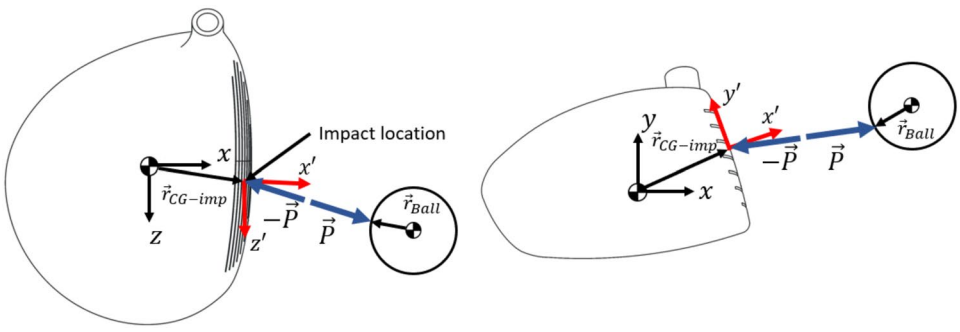

Fig. 1 Free body diagrams of a driver clubhead and ball

and is denoted by the subscript i. In Eqs. 3 and 4 the initial momenta are zero as the ball is at rest.

To solve for the 15 unknowns, three more equations are needed. Equation 5 imposes a COR of 0.83 along the x' axis, which is the maximum allowed by the USGA and R &A equipment rules [7]. COR is defined as the ratio between the relative velocity after the collision to the relative velocity before the collision.

$$e = \frac{-\left(\vec{\mathbf{v}}_{\mathbf{imp,c_f}} - \vec{\mathbf{v}}_{\mathbf{imp,b_f}}\right) \cdot \hat{\mathbf{i}}'}{\left(\vec{\mathbf{v}}_{\mathbf{imp,c_i}} - \vec{\mathbf{v}}_{\mathbf{imp,b_i}}\right) \cdot \hat{\mathbf{i}}'} \tag{5}$$

In Eq. 5, $\hat{\mathbf{i}}'$ is the unit vector parallel to x'. The subscript 'imp' denotes that these velocities are at the point of contact instead of the object's CG. These velocities are calculated using Eqs. 6 and 7, which are for rigid body motion.

$$\vec{\mathbf{v}}_{\mathbf{imp,c}} = \vec{\mathbf{v}}_{\mathbf{c}} + \vec{\boldsymbol{\omega}}_{\mathbf{c}} \times \vec{\mathbf{r}}_{\mathbf{CG-imp}} \tag{6}$$

$$\vec{\mathbf{v}}_{\mathbf{imp,b}} = \vec{\mathbf{v}}_{\mathbf{b}} + \vec{\boldsymbol{\omega}}_{\mathbf{b}} \times \vec{\mathbf{r}}_{\mathbf{ball}} \tag{7}$$

Lastly, Eqs. 8 and 9 impose a pure rolling condition of the ball on the clubface. This is applied by equating the ball and clubhead tangential velocity components after the collision.

$$\left(\vec{\mathbf{v}}_{\mathbf{imp,c_f}} - \vec{\mathbf{v}}_{\mathbf{imp,b_f}}\right) \cdot \hat{\mathbf{j}}' = 0 \tag{8}$$

$$\left(\vec{\mathbf{v}}_{\mathbf{imp,c_f}} - \vec{\mathbf{v}}_{\mathbf{imp,b_f}}\right) \cdot \hat{\mathbf{k}}' = 0 \tag{9}$$

This produces a set of 15 scalar equations to solve for the final impulse $\vec{\mathbf{P}}$ and velocity components of the ball and clubhead. Most IM-based models follow a similar construction. Winfield and Tan developed an IM model that represents the clubhead using a 3D ellipsoid, done to capture the curvature of a driver's clubface [8]. Penner proposed an IM-based driver model with flat clubface geometry [9]. Danaei et al. proposed an IM model that used a torus to represent the bulge and roll radii of a driver [10]. In this paper, toroidal geometry is used for the driver, while the iron models use a planar geometry for the clubface.

2.1.1 Adjusted IM model

The model proposed by Danaei et al. makes two adjustments to IM model parameters to improve accuracy [10]. First, a small amount of mass is added to the clubhead at its CG. The authors found that this reduced ball speed error without affecting spin. The authors hypothesised this additional mass compensates for neglecting the shaft [10]. The second adjustment is a small translation to the ball's center of gravity (CG). The authors found that moving the CG slightly downwards improved spin accuracy [10]. This adjustment represents deformations of the ball during impact. The original paper outlines an optimization approach to identify these adjustments using experimental data. An objective function was created that reduced the mean square error for the linear and angular velocities of the ball [10].

To implement this model, here the equations presented in Sect. 2.1 are applied and the additional clubhead mass is added to the parameter m_c. The adjustment to the ball CG is achieved by changing $\vec{\mathbf{r}}_{\mathbf{ball}}$, which is the vector from the ball's CG to the point of impact. This gives four parameters (m_c and three components of $\vec{\mathbf{r}}_{\mathbf{ball}}$) to be optimized during parameter identification. The optimization method and objective function used is outlined in Sect. 2.3.

2.1.2 Variable slip model

Cross and Dewhurst introduced a non-dimensional quantity referred to as the "horizontal coefficient of restitution" [11]. This parameter allows for a certain amount of slip to occur at the point of contact. Here it will be referred to as a slip ratio to avoid confusion with the standard COR term. This replaces the pure rolling assumption used by conventional IM-based models. The original model was derived for 2D impacts. Here the model is extended to predict 3D impacts. Refering to the model outlined in Sect. 2.1, Eqs. 8 and 9 are modified to allow a prescribed amount of slip between the clubhead and ball. This produces the following two equations to describe this behavior.

$$e_y = \frac{-\left(\vec{\mathbf{v}}_{\mathbf{imp,c_f}} - \vec{\mathbf{v}}_{\mathbf{imp,b_f}}\right) \cdot \hat{\mathbf{j}}'}{\left(\vec{\mathbf{v}}_{\mathbf{imp,c_i}} - \vec{\mathbf{v}}_{\mathbf{imp,b_i}}\right) \cdot \hat{\mathbf{j}}'} \tag{10}$$

$$e_z = \frac{-\left(\vec{\mathbf{v}}_{\mathbf{imp,c_f}} - \vec{\mathbf{v}}_{\mathbf{imp,b_f}}\right) \cdot \hat{\mathbf{k}}'}{\left(\vec{\mathbf{v}}_{\mathbf{imp,c_i}} - \vec{\mathbf{v}}_{\mathbf{imp,b_i}}\right) \cdot \hat{\mathbf{k}}'} \tag{11}$$

The numerator of Eq. 10 is the relative velocity between the ball and clubhead after impact, measured along the y' axis. Similarly, Eq. 11 is the relative velocity along the z' axis. Therefore, if e_y and e_z coefficients are set to zero, it is equivalent to a pure rolling condition.

From 2D experiments, the authors report slip ratio values ranging between −0.2 to 0.2 [11]. These values depend on the impact velocity, angle of incidence, coefficient of friction, and even the brand of the golf ball. For our 3D model, the slip ratio may be different in the horizontal and vertical directions as a golf club has a series of parallel grooves in the clubface. Therefore, the slip parameters e_y and e_z are left as parameters to be identified later.

2.2 Continuous models

Continuous impact models predict the time-varying contact forces and integrate the differential equations of motion to solve for positions and velocities during the impact. Therefore, the assumptions introduced for IM models are no longer imposed. In this section, three different contact models from the literature are extended to model 3D golf impacts. These models were developed in MapleSim, version 2022.1 (Maplesoft, Waterloo, Canada), which is a multibody dynamic simulation software. Custom components were developed to calculate the contact forces for each model.

2.2.1 Two-layer ball with volumetric contact model

The model proposed by McNally et al. [12] features a two-layer ball to capture the tangential force reversal observed in experimental studies. The inner core is connected to the outer cover with a rotary spring damper. The thickness of the outer layer (t_{cover}) is left as a parameter to be identified using optimization. The inner and outer components have mass and inertia properties assuming a uniform density. Additionally, the spring stiffness (k_{ball}) and damper rate (c_{ball}) are left as parameters to be optimized.

The model proposed by McNally et al. is unmodified for driver impacts. The normal force (F_{N}) is calculated using the volumetric contact model proposed by Gonthier and McPhee [13]. The volume of intersection (V) is calculated using two spheres to represent the curvature of a driver's clubface, shown in Fig. 2a. For modeling iron shots, the volume of intersection between a sphere and plane is used to represent a flat clubface as shown in Fig. 2b. To make the collision inelastic, a Hunt–Crossley damping term ($d\dot{x}$) is added as shown in Eq. 12.

$$F_{\text{N}} = k_V V + d_V \dot{x} k_V V \tag{12}$$

In Eq. 12, k_V is a stiffness parameter, d_V is the Hunt-Crossley damping parameter and $\dot{x}$ is the normal approach velocity. This equation is used for both driver and iron models.

Finally, the continuous velocity-based friction model proposed by Brown and McPhee [14] is used for the tangential force. In the model proposed by McNally et al [12], only the dynamic friction component is used. This gives Eq. 13 for the tangential force.

$$F_{\text{f}}(t) = F_{\text{N}} \mu \tanh\left(\frac{4\, v_{\text{t}}(t)}{v_{\text{tr}}}\right) \tag{13}$$

In Eq. 13, v_{t} is the instantaneous relative tangential velocity at the point of contact, μ is the dynamic coefficient of friction, and v_{tr} is the transition velocity. Above the transition velocity, this function behaves the same as Coulomb friction. Below the transition velocity, this function provides a gradual reduction in friction force. These parameters (μ & v_{tr}) are identified using optimization. The friction force, F_{f}, is applied to the ball and clubhead at the point of contact and is against the direction of relative tangential motion.

2.2.2 Concentric rings model applied to golf impacts

The model by Maw et al. [15] was originally developed for 2D oblique impacts of elastic spheres against a fixed plate. This model divides the contact area into a series of concentric rings. These rings can either grip (stick) to the surface or slip which captures the tangential force reversal behavior. In this section, two changes are made to make it more suitable for predicting golf impacts. First, the original model predicts perfectly elastic collisions using Hertzian contact theory. To model inelastic collisions, a Hunt–Crossley damping term is added to the normal force equation, as in the previous model . This produces Eq. 14.

$$F_{\text{N}} = kx^{\frac{3}{2}} + \mathrm{d}x^{\frac{3}{2}}\dot{x} \tag{14}$$

$$k = \frac{4G\sqrt{R}}{3(1-\nu)} \tag{15}$$

The first term in Eq. 14 is the original Hertzian normal force model. The second term is a hysteretic damping element that is proportional to the normal velocity ($\dot{x}$). The stiffness

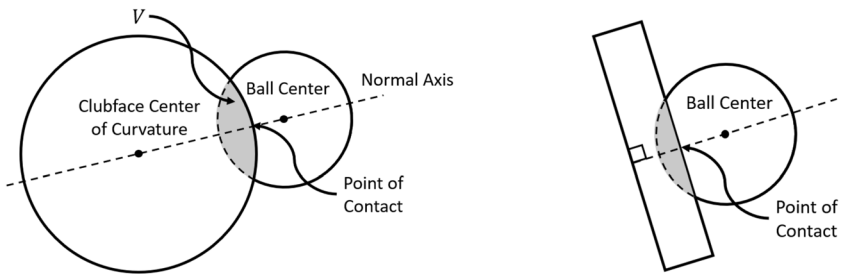

Fig. 2 Volume of intersection for normal force model

(a) Sphere-sphere volume of intersection. (b) Sphere-plane volume of intersection.

parameter, k, is derived from Hertzian contact theory and is shown in Eq. 15. G is the effective bulk modulus and ν is the effective Poisson's ratio. In Hertz's contact model, if both bodies are deformable, these properties can be lumped into a combined value. These material properties (d, G, ν) are left as parameters to be optimized later. Therefore, this model accounts for the deformation of both the golf ball and clubhead. In Eq. 15, R is the radius of the sphere. For the iron model, this is the radius of the ball. For the driver model, the equivalent radius is used to account for the curvature of the clubface. The equivalent radius is calculated using Eq. 16 [16]. It is assumed that the bulge and roll radii of the driver are the same and this value is used for r_{club}.

$$\frac{1}{r_{\text{eq.}}} = \frac{1}{r_{\text{ball}}} + \frac{1}{r_{\text{club}}} \tag{16}$$

The second change required is due to the original Maw model being derived for 2D collisions. To implement this as a 3D impact model, a 2D normal-tangential frame is assigned as shown in Fig. 3. The origin of this frame is at the point of contact on the clubface. The tangential axis is along the direction of relative motion between the ball and clubhead. The modified normal force is applied along the normal axis. The tangential force is calculated in the same manner as a 2D impact (Eq. 13) using the relative velocity at the point of contact. Using Newton's third law, these contact forces are reversed and applied to the clubhead as well.

2.2.3 Contact area model extended for golf impacts

Arakawa et al. [17] proposed that tangential force is a function of normal force and the time derivative of the contact area A (Eq. 17). This model was originally developed for 2D oblique impacts. Like the Maw model, a normal tangential frame is prescribed at the point of contact. The tangential force model is applied along the tangential axis.

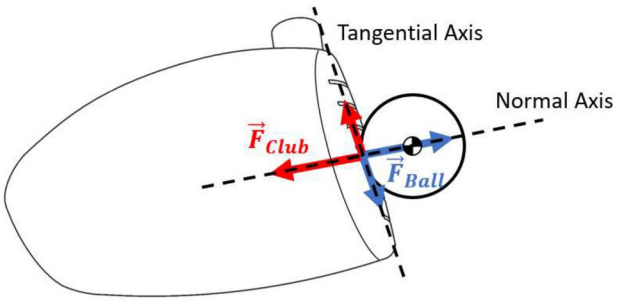

Fig. 3 Diagram showing the normal and tangential axis reference frame

$$F_{\text{T}} = \eta F_{\text{N}} + \eta\lambda \frac{\text{d}A}{\text{d}t} \tag{17}$$

To calculate $\frac{\text{d}A}{\text{d}t}$, Arakawa et al. used experimental measurements of the contact area. To create a predictive impact model, another model is required for the contact area and normal force. In this paper, Hertzian contact theory is used for the normal force and the contact area. Therefore, Eqs. 14 and 15 from Sect. 2.2.2 are applied here. This includes a Hunt–Crossley damping coefficient (d) to make the collision inelastic. From Hertzian contact theory the contact radius, b, is given by Eq. 18.

$$b = \sqrt{Rx} \tag{18}$$

In Eq. 18, R is the radius of the ball and x is the normal approach distance. Therefore, assuming the circular contact area can be expressed as:

$$A = \pi b^2 = \pi Rx \tag{19}$$

Taking the time derivative of this equation gives:

$$\frac{\text{d}A}{\text{d}t} = \pi R\dot{x} \tag{20}$$

Equation 20 shows that the time derivative of the contact area is proportional to the normal approach velocity according to Hertzian contact theory. Therefore, the tangential force expression proposed by Arakawa et al. can be written as:

$$F_{\text{T}} = \eta F_{\text{N}} + \eta\lambda\, \pi R\dot{x} \tag{21}$$

In Eq. 21, λ and η are contact parameters. This equation is used here to predict the tangential force. To create a 3D free clubhead model, a normal-tangential frame is used as outlined in Sect. 2.2.2.

2.3 Experimental validation

Experimental data was collected by a golf equipment manufacturer and shared with the University of Waterloo for this purpose (Ethics #41427). The equipment manufacturer wishes to remain unidentified and for individual golf swing data to not be shared publicly. The data consists of 550 drives and 120 7-iron shots by elite golfers. 56 participants with a scratch or better handicap index were used for testing. The golf shots were recorded with an 8 camera motion capture system operating at 720 Hz (Nexus, Vicon, Oxford, UK). This system measured the club kinematic data. The launch conditions of the ball were recorded using a commercial launch monitor (GC2, Foresight Sports, San Diego, CA, USA). The clubhead velocity and position were linearly extrapolated to estimate the conditions at the moment of impact, which were used as the initial states for the impact

models. This data was used to identify model parameters and evaluate the accuracy of these models. The physical properties of both clubheads and the golf ball are provided in Table 1. While this experiment could have been conducted with a mechanical swing robot, repeatable golf shots are not required. The purpose of these models is to predict the ball trajectory using the clubhead kinematics before impact.

The impact models discussed in the previous sections have unique parameters that affect the predicted launch conditions. An optimization approach was used to identify these parameters. Equation 22 is the cost function that was minimized:

$$C = \sum_{i=1}^{5} \left[\sum_{j=1}^{n} \frac{1}{n} \frac{|x_{\mathrm{Sim},i,j} - x_{\mathrm{Exp},i,j}|}{\mathrm{mean}(x_{\mathrm{Exp},i,1} : x_{\mathrm{Exp},i,n})} \right] \tag{22}$$

where $x_{\mathrm{Sim},i,j}$ are the simulated launch conditions of the ball and $x_{\mathrm{Exp},i,j}$ are the measured experimental values; j indicates the launch conditions for a particular shot of n total shots. The index i is for each launch condition, which has five values: ball speed, vertical launch angle, horizontal launch angle, backspin, and sidespin. The numerator of Eq. 22 is the absolute difference between the simulated launch condition and the experimental measurement. This is divided by the experimental mean to balance the weighting of each error term. The full data set was used in this optimization process.

Due to the non-linearity of the problem a hybrid optimization approach is used. First, a genetic algorithm (MATLAB, 2021B) is used to thoroughly search the solution space. A population of 200 and 100 generations was chosen for this step. The top five results from the last population are further optimized using fmincon (MATLAB 2021b). The best result from this process is used as the model parameters in the next section.

3 Results

The accuracy of these models is evaluated by comparing the predicted ball velocity after impact with the measured launch conditions. The mean absolute error (MAE) and standard deviation (STD) are considered to determine the best models. Since the magnitude of these values are different between driver and 7-iron shots, the relative errors are considered to compare the models.

Table 2 compares and summarizes the accuracy of the IM-driver models. The first column shows the experimental mean across all participants. The percent error relative to the experimental mean is shown in parentheses. The italicized regions in Table 2 shows the impact model with the least MAE for each respective launch condition. Table 2 also shows the average CPU time for 10 simulations using a single processor core with a 2.3 GHz clock rate. Table 3

Table 1 Properties of the clubheads and ball

Parameter	Driver	7-Iron	Description
m_c	204	264	Mass of the clubhead (g)
$\vec{r}_{\mathrm{CG-CF}}$	$\begin{bmatrix} 40.8 & 11.4 & 1 \end{bmatrix}$	$\begin{bmatrix} 3.61 & 4.85 & 1.12 \end{bmatrix}$	Vector from CG to centre of the clubface in *xyz* frame (mm)
I_{club}	$\begin{bmatrix} 2843 & -733 & 530.2 \\ -733 & 5679 & 0.5 \\ 530.2 & 0.5 & 4085 \end{bmatrix}$	$\begin{bmatrix} 2752 & -51 & -53 \\ -51 & 2889 & -429 \\ -53 & -429 & 576.6 \end{bmatrix}$	Clubhead inertia dyadic about the clubheads' CG (g cm^2)
Loft	9.8	30.5	Loft angle (°)
Bulge	305	∞	Bulge radius (mm)
Roll	305	∞	Roll radius (mm)
m_{ball}	45.9	45.9	Mass of the ball (g)
r_{ball}	21.3	21.3	Radius of the ball (mm)
I_{ball}	$83.36 I_{3\times3}$	$83.36 I_{3\times3}$	Inertia matrix of the ball (g cm^2)

Table 2 Mean experimental value, mean absolute error, standard deviation and average CPU time per simulation for the driver IM models

	Adjusted IM model			Variable slip model	
Ball	Exp.	MAE	STD	MAE	STD
Speed (mph)	158.9	*1.51 (0.95%)*	*1.27 (0.81%)*	1.85 (1.17%)	1.37 (0.86%)
Launch (°)	14.5	*0.68 (4.68%)*	*0.50 (3.45%)*	0.71 (4.90%)	0.48 (3.31%)
Azimuth (°)	2.19	*0.78 (35.6%)*	*0.49 (22.4%)*	0.81 (37.5%)	0.48 (21.9%)
Backspin (rpm)	2980	*211 (7.15%)*	*257 (8.62%)*	219 (7.50%)	266 (8.92%)
Sidespin (rpm)	490	153 (31.2%)	188 (38.3%)	*149 (30.2%)*	*176 (35.7%)*
Avg. CPU time	5.52 ms			5.68 ms	

compares and summarizes the accuracy of the continuous driver models. The experimental mean is not shown here because it is the same as table 2 as the same data set is used.

Table 4 compares and summarizes the accuracy of the IM-based 7-iron models. This table shows the mean absolute error and standard deviation between the predicted and measured ball launch conditions. Table 4 also shows the experimental mean for each launch condition which is used to calculate the relative error. Similarly, table 5 compares and summarizes the accuracy of the continuous 7-iron models. Once again the italicized regions in these tables show the impact model with the least MAE for each respective launch condition.

4 Discussion

In this paper new 3D impact models were developed and evaluated to determine which models have the highest accuracy for specific clubs. Additionally, the computation times of these models are compared as this may be important for certain applications. While the azimuth and sidespin errors are relatively high, the magnitude of these errors are similar to the other measures. Furthermore, a portion of the model error can be attributed to the accuracy of commercial launch monitor devices. While the manufacturer does not report the accuracy, through independent testing, the mean spin error is about 50 rpm and the launch direction error is about 0.2° [18]. Therefore, near zero error is impossible with this data set; thus, we concluded the model with the lowest error performs the best.

First, the different driver impact models are examined. From Table 2, the adjusted IM model results in less ball speed error compared to the variable slip model. This is mainly attributed to the additional clubhead mass that increased ball speed for all shots. In the original paper, Danaei et al. suggested that this additional mass was to compensate for neglecting the shaft. Comparing the other launch conditions reveals similar accuracy between these models. Finally, Table 2 shows the average CPU time for a single simulation. This is expected as the system of equations is

Table 3 Mean absolute error, standard deviation and average CPU time per simulation for the driver continuous models

	Volumetric model		Rings model		Area model	
Ball	MAE	STD	MAE	STD	MAE	STD
Speed (mph)	*2.12 (1.33%)*	*2.91 (1.83%)*	2.27 (1.43%)	3.07 (1.93%)	2.29 (1.44%)	3.12 (1.96%)
Launch (°)	0.54 (3.72%)	0.55 (4.00%)	*0.52 (3.72%)*	*0.55 (4.00%)*	0.76 (5.24%)	0.86 (5.93%)
Azimuth (°)	*1.07 (48.8%)*	*0.52 (23.7%)*	1.13 (51.6%)	0.52 (23.7%)	1.16 (53.0%)	0.54 (24.7%)
Backspin (rpm)	*228 (7.65%)*	*239 (8.02%)*	385 (12.9%)	356 (11.9%)	634 (21.3%)	582 (19.5%)
Sidespin (rpm)	*227 (46.3%)*	*252 (51.4%)*	298 (60.8%)	334 (68.1%)	316 (64.4%)	348 (71.0%)
Avg. CPU time	0.683 s		1.46 s		0.586 s	

Table 4 Mean experimental value, mean absolute error, standard deviation, and average CPU time per simulation for the 7-iron IM models

	Adjusted IM model			Variable slip model	
Ball	Exp.	MAE	STD	MAE	STD
Speed (mph)	117.0	*2.31 (1.97%)*	*2.28 (1.95%)*	2.86 (2.44%)	2.49 (2.13%)
Launch (°)	18.9	1.12 (5.93%)	0.99 (5.24%)	*1.06 (5.12%)*	*1.04 (5.50%)*
Azimuth (°)	2.19	*0.86 (39.3%)*	*0.53 (24.2%)*	0.94 (42.9)	0.58 (26.5%)
Backspin (rpm)	6487	*563 (8.75%)*	*363 (5.53%)*	583 (8.99%)	373 (5.75%)
Sidespin (rpm)	681	*340 (49.8%)*	*250 (36.7%)*	352 (51.7%)	260 (38.1%)
Avg. CPU time		6.04 ms		6.24 ms	

Table 5 Mean absolute error, standard deviation and average CPU time per simulation for the 7-iron continuous models

	Volumetric model		Rings Model		Area Model	
Ball	MAE	STD	MAE	STD	MAE	STD
Speed (mph)	2.42 (2.06%)	1.65 (1.41%)	*2.26 (1.93%)*	*1.61 (1.38%)*	3.33 (2.85%)	2.17 (1.85%)
Launch (deg)	*0.77 (4.07%)*	*0.88 (4.66%)*	1.52 (8.04%)	1.06 (5.61%)	1.63 (8.63%)	0.94 (4.97%)
Azimuth (deg)	*0.70 (32.0%)*	*0.48 (21.9%)*	0.73 (33.3%)	0.46 (21.0%)	0.82 (37.4%)	0.49 (22.4%)
Backspin (rpm)	*436 (6.72%)*	*272 (4.19%)*	653 (10.0%)	477 (7.35%)	998 (15.4%)	953 (14.7%)
Sidespin (rpm)	363 (53.3%)	256 (36.6%)	*358 (52.6%)*	*245 (35.9%)*	403 (59.2%)	297 (43.6%)
Avg. CPU time	0.721 s		1.59 s		0.635 s	

similar. Overall the adjusted model is the best IM-based model for predicting driver impacts.

Table 3 compares and summarizes the accuracy of the continuous driver models. The two-layer ball volumetric model performed the best overall of the continuous driver models considered. All launch conditions have the lowest error except for the vertical launch angle, which is slightly improved with the concentric rings model. The contact area model had the highest errors of the group. Table 3 also shows the average CPU time. The concentric rings model requires the most amount of compute time. The volumetric and area models demonstrated similar compute times.

Comparing Tables 2 and 3 reveals that the adjusted IM model is overall the most accurate of the models considered for driver impacts. Interestingly, the volumetric and concentric rings model performed slightly better for predicting the launch angle. The remaining launch conditions are all in favour of the adjusted IM model. Comparing the average CPU times in Tables 2 and 3 shows that the adjusted IM model required less time by two orders of magnitude compared to the continuous models. This is expected, as the continuous models need to calculate hundreds of positions and velocities throughout the duration of the impact.

Next, the different 7-iron models are examined. From Table 4, the adjusted IM model results in less ball speed error compared to the variable slip model. Again, this is attributed to the additional clubhead mass that increases ball speed for all shots. Vertical launch angle is improved with the variable slip model. However, the remaining launch conditions are in favour of the adjusted IM model. The average CPU time per simulation is similar to the driver models.

Table 5 compares and summarizes the accuracy of the continuous 7-iron models. The concentric rings model demonstrated the best accuracy for ball speed and sidespin, while the two-layer ball volumetric model is the best for the remaining launch conditions. Overall, the volumetric model is the most accurate of the continuous models as it results in the lowest cost function value. Again, the contact area model demonstrated significantly less accuracy than the other models considered. Finally, comparing the CPU times reveals similar trends to the driver models.

Comparing Tables 4 and 5 reveals that the concentric rings model has the least ball speed error and the adjusted IM-model has the least sidespin error. The two-layer ball volumetric model is more accurate for the remaining launch conditions. During the optimization process, the adjusted IM model returned a cost function value of 1.05 and the volumetric model returned a value of 0.98. Therefore, only considering accuracy, the volumetric model is the best overall for predicting a 7-iron shot. Comparing the average CPU times in Tables 4 and 5 shows that the IM models require two orders of magnitude more compute time compared to the continuous models.

Table 6 Optimized adjusted IM model parameters

Parameter	Driver	7-Iron
Δ Mass (g)	2.54	10.10
$\Delta\,\mathrm{CG}_{\mathrm{Ball}}$ (mm)	(0, − 0.482, − 0.068)	(− 0.395, − 0.182, − 0.071)

Table 7 Optimized variable slip IM model parameters

Parameter	Driver	7-Iron
e_y	− 0.0103	0.0183
e_z	− 0.0150	0.0423

Table 8 Optimized 2-layer volumetric model parameters

Parameter	Driver	7-Iron
$K_{\mathrm{v}}\left(\frac{\mathrm{N}}{\mathrm{N}^3}\right)$	6.25×10^9	6.83×10^9
$d_{\mathrm{v}}\left(\frac{\mathrm{ms}}{\mathrm{m}}\right)$	6.42	9.26
μ	0.372	0.489
$k_{\mathrm{Ball}}\left(\frac{\mathrm{Nm}}{\mathrm{rad}}\right)$	13.5	34.1
$c_{\mathrm{Ball}}\left(\frac{\mathrm{ms}}{\mathrm{rad}}\right)$	2.53	13.2
t_{cover} (mm)	1.26	2.55
v_{tr} (m/s)	0.936	0.812

Table 9 Optimized parameters for concentric rings model

Parameter	Driver	7-Iron
G (GPa)	5.58	5.74
ν	0.407	0.418
$d\left(\frac{\mathrm{ms}}{\mathrm{m}}\right)$	6.50	11.5
μ	0.360	0.519

Table 10 Optimized parameters for contact area model

Parameter	Driver	7-Iron
G (GPa)	5.40	5.24
ν	0.398	0.412
$d\left(\frac{\mathrm{ms}}{\mathrm{m}}\right)$	6.35	9.89
η	1.32×10^5	2.06×10^5
λ	0.0486	0.118

Finally, since only elite golf swings were used for parameter identification, the accuracy reported in this paper is representative for swings with similar clubhead kinematics. For example, clubhead speed for the driver data set varies from

101 to 118 mph. Predicting swings outside of this range may result in reduced accuracy and require additional parameter tuning.

5 Conclusion

Five impact models were developed and tuned to predict the 3D collision between a golf clubhead and ball: adjusted IM, variable slip, 2-layer-ball volumetric, concentric rings, and area model. These models were validated and compared using experimental data for driver and 7-iron shots. It was found that impact models developed and validated for drivers can be applied to iron type clubs and achieve similar accuracy. It was observed that the adjusted IM model proposed by Danaei et al performed the best overall out of the driver models considered. For predicting a 7-iron shot, the two-layer ball volumetric model demonstrated the best accuracy. However, IM-based models still performed well for iron shots while requiring two orders of magnitude less compute time than continuous models. These models can be helpful for club design, club fitting and to understand the relationship between club delivery and ball flight.

Appendix: Optimized model parameters

This appendix contains the optimized parameters for the impact models presented throughout this paper. Each table show the parameters for both the driver and 7-iron clubs. Table 6 shows the optimized model parameters for the adjusted IM model described in Sect. 2.1.2.

Table 7 shows the optimized parameters for the variable slip IM-based model described in Sect. 2.2

Table 8 shows the optimized model parameters for the two-layer volumetric model described in section 2.2.1.

Table 9 shows the optimized model parameters for concentric rings model described in Sect. 2.2.2.

Table 10 shows the optimized model parameters for the contact area model described in Sect. 2.2.3.

Data Availability The equipment manufacturer wishes to remain unidentified and for individual golf swing data to not be shared publicly.

Declarations

Conflict of Interest The authors declare no Conflict of interest.

References

1. PGA Tour Statistics. https://www.pgatour.com/content/pgatour/stats/. Accessed April 2023 (2022)
2. Cochran A (2002) The impact of science and technology on golf equipment-personal view. Eng Sport 4:3–15
3. McPhee J (2022) A review of dynamic models and measurements in golf. Sports Eng 25:22
4. Petersen W, McPhee J (2009) Shape optimization of golf clubface using finite element impact models. Sports Eng 12:77–85. https://doi.org/10.1007/s12283-009-0030-7
5. Leach RJ, Forrester SE, Mears AC, Roberts JR (2017) Design optimization of golf clubhead and ball with numerical analysis. Glob J Res Eng 17:23–29
6. Cochran AJ, Stobbs J (1968) The search for the perfect swing. Morrison & Gibb Ltd, London
7. The Equipment Rules, The USGA and R &A (2019). https://www.usga.org/content/dam/usga/pdf/Equipment/Equipment%20Rules%20Final.pdf. Accessed April 2023
8. Winfield DC, Tan TE (1994) Optimization of clubhead loft and swing elevation angles for maximum distance of a golf drive. Comput Struct 53(1):19–25. https://doi.org/10.1016/0045-7949(94)90125-2
9. Penner AR (2001) The physics of golf: the convex face of a driver. Am J Phys 69(10):1073–1081. https://doi.org/10.1119/1.1380380
10. Danaei B, McNally W, Henrikson E, McPhee J (2020) Adjusting a momentum-based golf clubhead-ball impact model to improve accuracy. Proceedings, 2018, 49(1):47. https://doi.org/10.3390/proceedings2020049047
11. Cross R, Dewhurst P (2018) Launch speed, angle and spin in golf. Eur J Phys 39(6):065003. https://doi.org/10.1088/1361-6404/aadda8
12. McNally W, McPhee J, Henrikson E (2018) The golf shaft's influence on clubhead-ball impact dynamics. Proceedings, 2018, 2(6):246. https://doi.org/10.3390/proceedings2060245
13. Boos M, McPhee J (2013) Volumetric modeling and experimental validation of normal contact dynamic forces. J Comput Nonlinear Dyn 8(2):021006. https://doi.org/10.1115/1.4006836
14. Brown P, McPhee J (2016) A continuous velocity-based friction model for dynamics and control with physically meaningful parameters. J Comput Nonlinear Dyn 11(5):054502. https://doi.org/10.1115/1.4033658
15. Maw N, Barber JR, Fawcett JN (1976) The oblique impact of elastic spheres. Wear 38(1):101–114. https://doi.org/10.1016/0043-1648(76)90201-5
16. Jackson RL, Ghaednia H, Lee H, Rostami A, Wang X (2013) Contact mechanics. In: Tribology for scientists and engineers: from basics to advanced concepts. Springer, New York, NY. https://doi.org/10.1007/978-1-4614-1945-7/3
17. Arakawa K, Mada T, Komatsu H, Shimizu T, Satou M, Takehara K, Etoh G (2009) Dynamic deformation behavior of a golf ball during normal impact. Exp Mech 49(4):471–477. https://doi.org/10.1007/s11340-008-9156-y
18. Leach RJ, Forrester SE, Mears AC, Roberts JR (2017) How valid and accurate are measurements of golf impact parameter obtained using commercially available radar and stereoscopic optical launch monitors? Measurement 112:125–136. https://doi.org/10.1016/j.measurement.2017.08.009